Science Bulletin 64 (2019) 1285–1292

Contents lists available at ScienceDirect

Science Bulletin

journal homepage: www.elsevier.com/locate/scib

Science Bulletin
www.scibull.com

Article

Near-infrared emissive carbon dots with 33.96% emission in aqueous solution for cellular sensing and light-emitting diodes

Boyang Wang [a], Jian Li [a], Zhiyong Tang [b,c], Bai Yang [d], Siyu Lu [a,b,*]

[a] College of Chemistry, Zhengzhou University, Zhengzhou 450001, China
[b] Henan Institute of Advanced Technology, Zhengzhou University, Zhengzhou 450001, China
[c] CAS Key Laboratory of Nanosystem and Hierarchical Fabrication, CAS Center for Excellence in Nanoscience, National Center for Nanoscience and Technology, Beijing 100190, China
[d] State Key Laboratory of Supramolecular Structure and Materials, College of Chemistry, Jilin University, Changchun 130012, China

ARTICLE INFO

Article history:
Received 20 June 2019
Received in revised form 8 July 2019
Accepted 11 July 2019
Available online 19 July 2019

Keywords:
Carbon dots
Fluorescence
Red emission
Aqueous
Cellular sensing

ABSTRACT

Near-infrared emissive carbon dots (CDs) were synthesized by hydrothermal method. The as-prepared CDs exhibited a relatively high quantum yield (QY) of 33.96% in an aqueous solution, and the peak toward the near-infrared fluorescence reached 685 nm. The CDs exhibited pH-sensitive characteristics under strong acidic conditions. Even at pH = 0, the as-prepared CDs retained a high fluorescence intensity, which proved that they possessed good acid resistance. More importantly, the CDs were sensitive to the Fe^{3+} changes in living cells. In addition, they could also be used for white and red emissive LEDs. This discovery will expand the use of aqueous-phase high QY CDs in the field of living cell sensing and imaging.

1. Introduction

Carbon dots (CDs) have attracted much attention recently due to its excellent physical chemical and optical properties [1–4], low amounts of photobleaching, low cytotoxicity and excellent biocompatibilities [5,6], unlike traditional semiconductor quantum dots, such as those based on CdX (X = S, Se, Te) [7–9]. Nowadays CDs have been widely used for bioimaging, detection probes, drug delivery, and optoelectronic devices [10–14].

At present, most of the known CDs produce blue to green emissions with ultraviolet or blue excitation, which limits their multi applications [15–18]. The development of more environmentally friendly synthesis methods for the efficient and controllable preparation of red-emitting CDs with high quantum yields in aqueous solutions is crucial [19–21]. Red fluorescence emitting materials are favorable for many applications, particularly in the biomedical fields, because blue light and ultraviolet light usually cause damage to biological tissues [22,23]. Since the discovery of CDs, researchers have explored a variety of synthesis pathways to prepare CDs from a variety of carbon sources, such as arc discharge, laser ablation [24,25], electrochemical synthesis [26,27], microwave [28,29], acidic oxidation, solvothermal methods [30,31], and hydrothermal methods [32–35]. Among these, hydrothermal and solvothermal methods are environmentally friendly and economical synthesis methods because the as-prepared CDs do not require further passivation. Through these methods, hydrophilic groups, such as a hydroxyl or carboxyl groups, are generated on the surface of CDs, which is convenient for subsequent applications [36,37]. Hydrophilic groups can increase the water dispersity of the CDs, facilitating cell and biological experiments. The surface carboxyl groups may interact with certain metal ions to cause fluorescence quenching, allowing the detection of specific metal ions [38–43]. As the name implies, the reaction solvent used in hydrothermal reactions is water, and the reaction solvent used in the solvothermal treatment is an organic substance, such as ethanol, dichloromethane, or DMF. Thus, the hydrothermal method is less harmful to the human body during the synthesis process and more in line with the principle of green chemistry.

Therefore, in recent years, many scientists have been working on the preparation of red emissive CDs in aqueous solution. There have been many types of red emissive CDs synthesized, but most of them were formed using solvothermal methods [44–49]. Red emissive CDs prepared by hydrothermal methods have been rarely reported [50]. Liu et al. [51] prepared red emissive CDs by the hydrothermal treatment of 2,5-diaminobenzenesulfonic acid and 4-aminophenylboronic acid hydrochloride. When excited by 500 nm wavelength, the best emission intensity is obtained, and the maximum emission wavelength is 600 nm (quantum yield

* Corresponding author.
E-mail address: sylu2013@zzu.edu.cn (S. Lu).

https://doi.org/10.1016/j.scib.2019.07.021
2095-9273/

(QY) = 5.44%). Gao et al. [52] synthesized red emissive CDs by the hydrothermal treatment of citric acid and neutral red. The solution of CDs exhibited a QY of 12.1%. Liu et al. [53] used o-phenylenediamine to prepare red emissive CDs, with QY of 10.83% in water and 31.54% in ethanol.

It is critical to continue to develop water dispersity and long-wavelength red emissive CDs with high quantum yields while maintaining their properties and advantages in different solvents. However, the red emissive CDs prepared by hydrothermal methods often exhibit low quantum yields, while the red emissive CDs prepared by solvothermal are often quenched in aqueous solution, which greatly limits the application of red emissive CDs. According to our previous work, we designed a red emissive CDs with a maximum emission peak of 685 nm by hydrothermal method, which has a high quantum yield in aqueous solution.

Herein, we designed a hydrothermal synthesis route using o-phenylenediamine and dopamine as raw materials to prepare red emissive CDs with high quantum yield in aqueous phase. The o-phenylenediamine and dopamine were not only the carbon source, but also provided amino functional group to make fluorescent CDs have better photostabilities. The synthesized CDs have the highest emission at 685 nm and exhibit no excitation dependence, and they possess a high absolute quantum yield (33.96%) in an aqueous solution. The as-prepared CDs underwent fluorescence quenching in the presence of Fe^{3+}, which would allow the CDs to be used as a sensitive detector of Fe^{3+} in living cells. Because of the simple synthesis method and excellent performance for various applications, the red emissive CDs synthesized in this study will advance the knowledge of CDs synthesis and living cell sensing and imaging applications.

2. Results and discussion

The morphologies and size distributions of CDs can be obtained using transmission electron microscopy (TEM). As shown in Fig. 1a, the as prepared CDs had uniformed quasi-spherical shapes and the average particle size was 5.6 nm (Fig. S1 online). From the high-resolution transmission electron micrograph, the lattice spacing of the CDs is 0.35 nm (Fig. 1b), which corresponds to the (0 0 2) crystal plane of the graphite carbon. The 26° that appeared in the X-ray diffraction (XRD) pattern was associated with a graphite structure and the (0 0 2) crystal plane of graphite carbon (Fig. 1c), which agrees with the TEM data [20]. Through Fourier-transform infrared spectroscopy (FTIR) and X-ray photoelectron spectroscopy (XPS), the chemical compositions and functional groups of the CDs can be evaluated. In the FTIR spectra (Fig. 1d), the peak at 3,411 cm^{-1} indicated the presence of —NH_2 or —OH; the peaks at 1,610 and 1,414 cm^{-1} attributed to the stretching vibrations of C=O, C=N, and C=C bonds, the peak at about 1,100 cm^{-1} was assigned to C—N stretching vibrations [16]. The XPS survey spectrum in Fig. 2a indicated that the CDs comprised C, O, and N elements with their contents 72.99%, 19.58%, 7.43% respectively. The high-resolution spectrum of C1s (Fig. 2b) can be decomposed into three peaks, the binding energy of 284.6 eV corresponds to C—C/C=C, 286.1 eV corresponds to C—N, C—O, and 288.3 eV corresponds to C=O. The N1s spectrum in Fig. 2c is compared to 398.5 (C—N—C), 399.3 (N— $(C)_3$), 400.1 eV (N—H). The high-resolution spectrum of O1s can be decomposed into two peaks with binding energies of 531.2 and 533.3 eV, respectively, corresponding to C=O and C—OH/C—O—C (Fig. 2d) [54]. The FTIR and XPS analysis above revealed that abundant hydrophilic functional groups not only provided interaction sites for specific ions or compounds but improved the dispersity. In our previous work, the CDs we prepared showed red emission in ethanol and did not show excellent fluorescent properties in aqueous solution. We have improved the experiment by replacing HCl with H_2SO_4, and the preparation method has changed from solvothermal to hydrothermal. In comparison with our previous work, it can be seen that the characteristic peak of the hydroxyl group in the infrared becomes less obvious in FTIR, and in the XPS, the proportion of oxygen element is improved, and the proportion of graphitized nitrogen is also improved [55]. N atoms can use their unpaired electrons to improve the emission properties of CDs. The energy

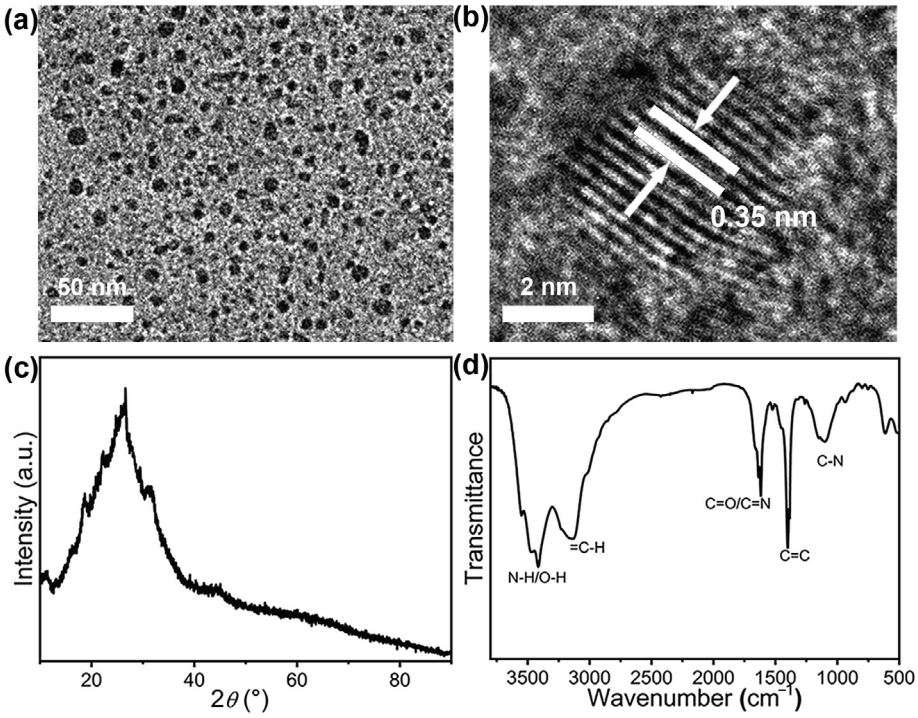

Fig. 1. Structural characterization of the sample. (a) TEM image, (b) HRTEM image of CDs, (c) XRD pattern, (d) FTIR spectrum, of CDs.

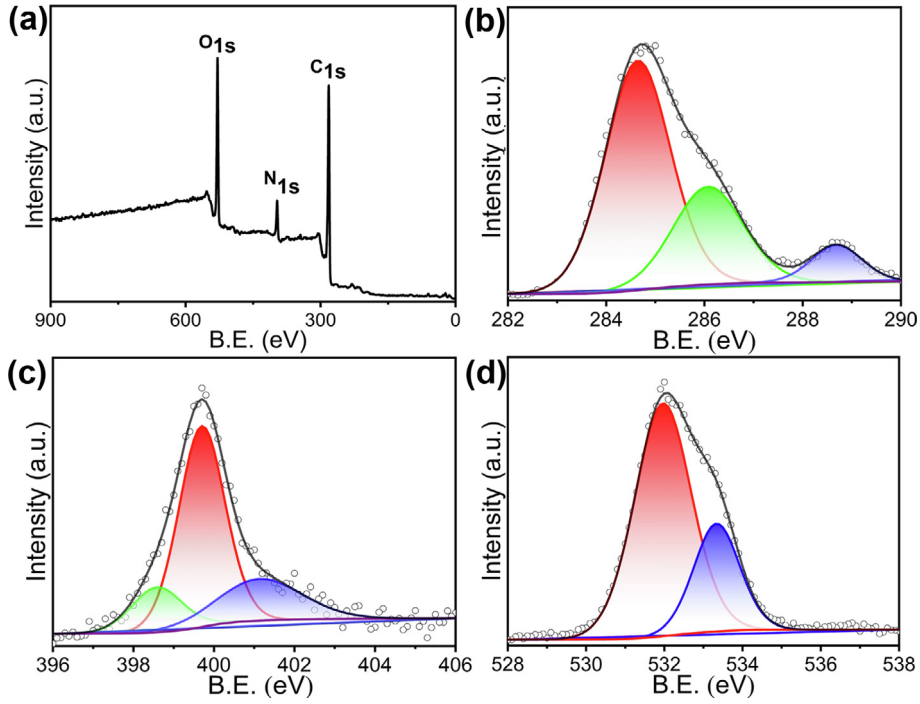

Fig. 2. XPS spectra of the sample (a) XPS survey spectrum and (b) C1s, (c) N1s, and (d) O1s high-resolution XPS spectra of the CDs (B.E.: binding energy).

gap adjustment in the CDs also depends on the N and O contents, while the oxygen-containing functional groups, particle size, and graphite nitrogen together determine the different fluorescence characteristics of these CDs [56]. In addition, H_2SO_4 also plays an important role in the reaction process. H_2SO_4 has a strong carbonization effect, which can promote the nucleation of CDs, and H_2SO_4 also has oxidative properties, which leads to an increase in the hydrophilicity of the surface of the CDs.

UV–vis absorption and fluorescence spectra of CDs were studied at room temperature. The aqueous solution showed three UV absorption peaks at 223, 280, and 615 nm (Fig. 3a). The absorption at 223 and 280 nm was attributed to the π–π* transition of the C═O bond and n-π* transition of the sp^2 aromatic domains, respectively. The peak at 615 nm may due to other functionalized surface groups of the CDs. When the aqueous CDs were excited at 560 nm, they exhibited strong fluorescence in the range of 570–800 nm,

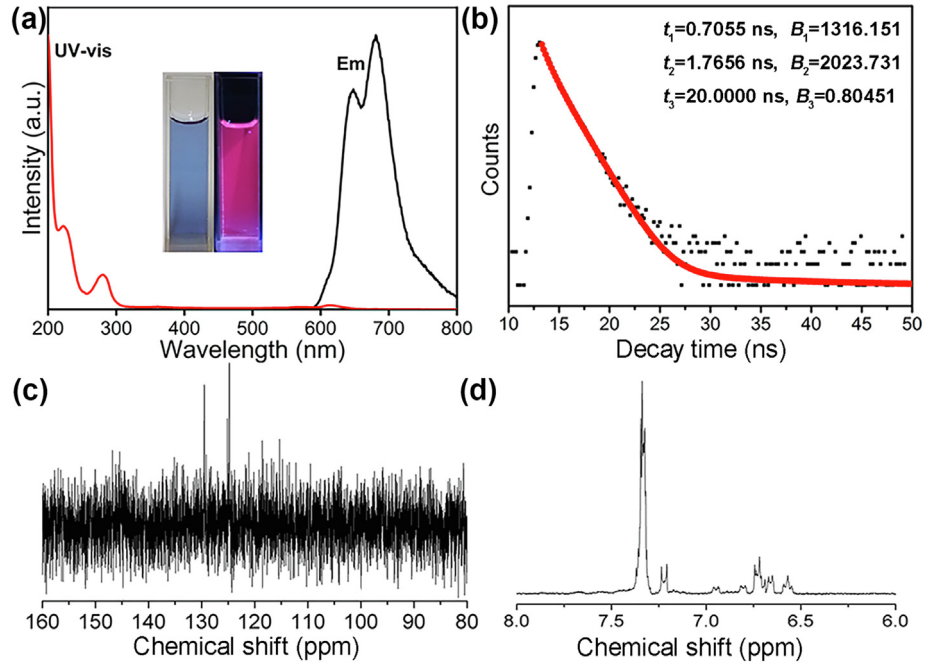

Fig. 3. (a) UV–vis absorption spectrum (red line) and fluorescence emission spectra (Em) (black line, λ_{ex} = 560 nm) of the CDs dispersed in water at room temperature. The insets show the photograph (left) and fluorescence image of the CDs solution under 365 nm light (right). (b) Decay time, (c) ^{13}C NMR spectrum, and (d) ^{1}H NMR spectrum of the CDs.

with two peaks at 648 and 685 nm and a maximum peak located at around 685 nm [21]. Furthermore, they exhibited obvious excitation-independent fluorescence (Fig. S2 online). The excitation-independent emission characteristics were attributed to surface chemical states and the homogeneous microstructures of the CDs, which caused them to exist uniformly in the lowest singlet state. Thus, the absolute QY was calculated to be 33.96% in aqueous solution by using integrating sphere. Furthermore, the fluorescence lifetime decay of the CDs was investigated [51]. As shown in Fig. 3b, the origin of fluorescence is studied by time-dependent single photon counting (TCSPC), which is an important technique to elucidate the excitation behavior of electrons. The insert shows that the long lifetimes over the whole emission spectra could be fit to three exponential components. The fluorescence behaviors were on a nanosecond timescale, indicating that the samples had only fluorescent properties, with the longest lifetime being 20 ns. Raman scattering reveals the structural characteristics of C atoms in CDs. As shown in Fig. S3 (online), the Raman spectrum of the CDs featuring two peaks corresponding to D bands and G bands. The intensity ratio of characteristic Raman bands (I_D/I_G) can be used to study the structural properties of carbon skeleton, especially the crystallinity and relative abundance of carbon core and surface atoms. I_D/I_G = 1.5, the possible reason is that the tiny graphitized CDs are embedded in some disordered carbon [57]. ^{13}C NMR spectra (Fig. 3c) show signals in the 120–140 ppm range, indicating sp^2 C atoms. If the electron-withdrawing or electron-releasing group (—NH_2) is introduced, the chemical shift of benzene at about 125.8 ppm will change. Therefore, these different signals also indicate that —NH_2 and aromatic rings form a conjugated polymer skeleton system. In addition, no signal was observed at the lower chemical shift (20–100 ppm), which corresponds to the sp^3 C atoms. In ^1H NMR spectroscopy (Fig. 3d), the signal of aromatic H can be detected in the range of 7.0–7.5 ppm, and 6.9 ppm active H signal from —NH— group can also be detected at 6.69 ppm [58].

The CDs (100 μL) were diluted in pure water solution (pH = 7.0) for the fluorescence measurements. The stabilities of CDs under different conditions were studied. The as-prepared CDs showed excellent photostabilities in fluorescence intensity, which remained invariant under continuous excitation (365 nm) with a UV lamp for 8 h (Fig. S4 online). The fluorescence intensity of the CDs only slightly changed, even when the pH values varied from 5 to 11 (Figs. S5 and S6 online), and there was a linear relationship when the pH was less than 4. By fitting the relative fluorescence intensities, there was a good linear relationship at pH values below 4, with an R^2 = 0.992 (Fig. S6 online). Meanwhile, the CDs exhibited low photobleaching and high storage stability after storing for 40 d (Figs. S6 and S7 online). These results indicated that the CDs possessed good stabilities and exhibited great potential for the design of fluorescence nanoprobes for complex matrices.

The CDs possessed good biocompatibilities and excellent light stabilities, and thus, they are an ideal material for bioimaging in biological applications (Fig. S8 online). We performed cell imaging experiments using light with 561 nm wavelength. Fig. 4a and 4b show the bright field images of AGS cells and the fluorescence images of AGS cells after adding CDs. It can be seen that AGS cells labeled with CDs showed bright red fluorescence under the excitation of 561 nm. Careful observation showed that CDs mainly dis-

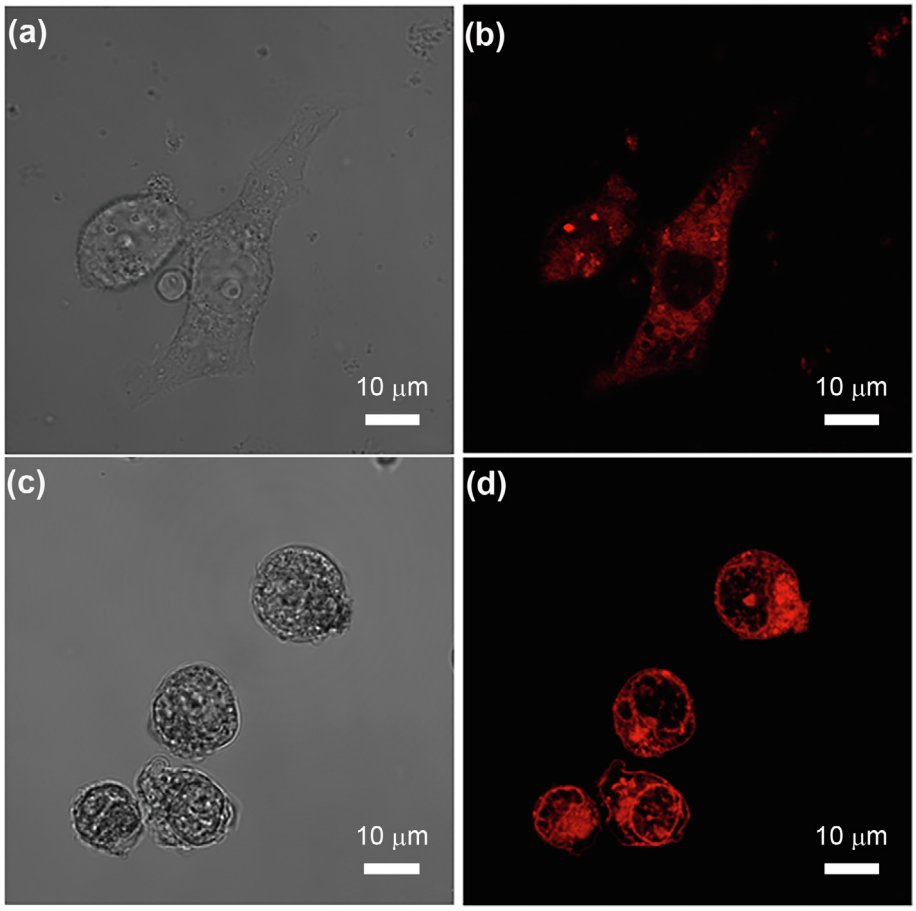

Fig. 4. CDs for bioimaging. (a), (b) Brightfield photomicrographs of the AGS cells incubated with CDs by excitation at 561 nm. (c), (d) Brightfield photomicrographs of the K562 cells incubated with CDs by excitation at 561 nm.

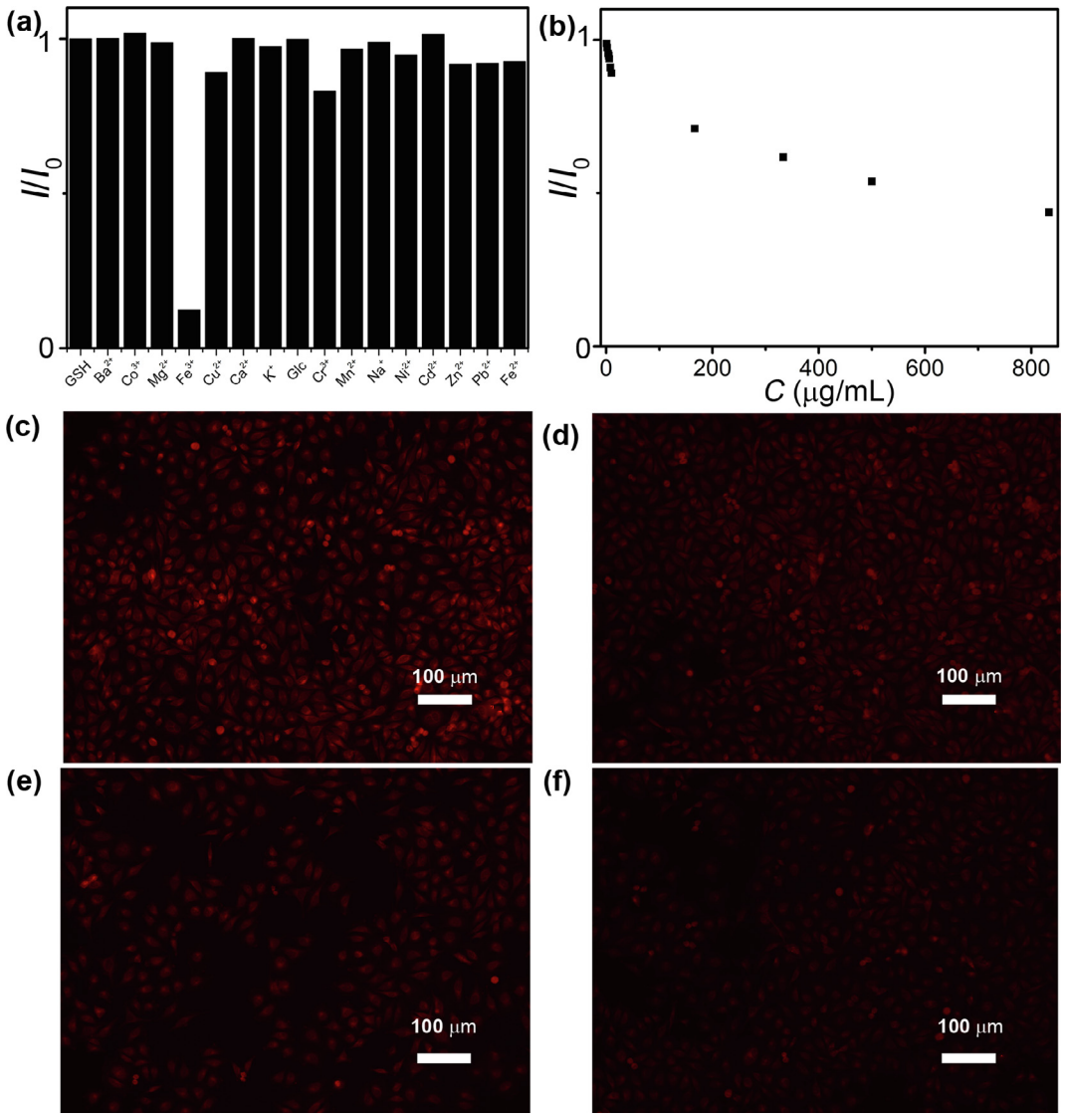

Fig. 5. CDs for Fe^{3+} detection. (a) The change in the fluorescence intensity at 685 nm of the CDs in the presence of various metal ions. (b) Effect of Fe^{3+} concentrations on the relative fluorescence intensity of the CDs. Overlaid confocal fluorescence images of living MGC-803 cells labelled with CDs under different conditions: (c) only CDs, (d) CDs + 50 μmol L^{-1} Fe^{3+}, (e) CDs + 100 μmol L^{-1} Fe^{3+}, and (f) CDs + 250 μmol L^{-1} Fe^{3+}.

tributed in the cytoplasmic region and could stain the cytoplasm and be confined outside the nucleus. To demonstrate this result, we tested another cell line, K562. The fluorescence image (Fig. 4d) reflects the bright red fluorescence of the cytoplasm in the cells when excited at the wavelength of 561 nm. More recent observations showed that CDs were mainly distributed in the cytoplasm, consistent with AGS cells. These results indicated that CDs can easily penetrate cell membrane and mark the cytoplasm, and thus, making it an ideal cell imaging agent. Inspired by the excellent properties of the probes, the cellular imaging abilities of the probes were explored.

The surface of the CDs contains oxygen and nitrogen functional groups which can interact with metal ions to form complex compounds by coordination, thus providing CDs with the potential to be used as fluorescent probes for detecting metal ions. Since the Fe^{3+} ion has a half-field 3d shell, which makes it a good electron acceptor, the fluorescence quenching by Fe^{3+} is believed to be related to the fast electron transfer process between Fe^{3+} and the CDs. Moreover, no electron transfer could occur between the CDs and Fe^{2+} ions, and thus, the quenching effect of Fe^{2+} is almost negligible. Firstly, 2 mmol L^{-1} solutions of various metal ions, including Ba^{2+}, Co^{3+}, Mg^{2+}, Fe^{3+}, Fe^{2+}, Cu^{2+}, Ca^{2+}, K^+, Cr^{3+}, Mn^{2+}, Na^+, Ni^{2+}, Cd^{2+}, Zn^{2+}, and Pb^{2+} ions, were added to the CDs' solutions, then excited with 560 nm, and recorded the fluorescence intensity at 685 nm (Fig. S9 online). From Fig. 5a, obvious fluorescence quenching effect was observed when 2 mol L^{-1} Fe^{3+} was added, while the effect of other metal ions could be neglected. The concentrations of Fe^{3+} ions were subsequently observed.

The relationship between the CDs fluorescence I/I_0 and Fe^{3+} concentration is linear in the 1–10 μmol L^{-1} Fe^{3+} range of concentration (Fig. 5b). The fluorescence intensity is given by the following equation: $I/I_0 = -0.01C + 1$, where I_0 and I are the fluorescent intensity of CDs before and after adding Fe^{3+}, and C represents the concentration of Fe^{3+}. This result agrees with the Stern–Volmer relationship after using the mathematical transformation: $I_0/I = 1 + K_{sv}C = 1 + 0.01217C$ (K_{sv} is the Stern-Volmer quenching constant) (Fig. S10 online). Next, we explored the response of CDs to changes in intracellular Fe^{3+} concentration. MGC-803 cells and CDs were

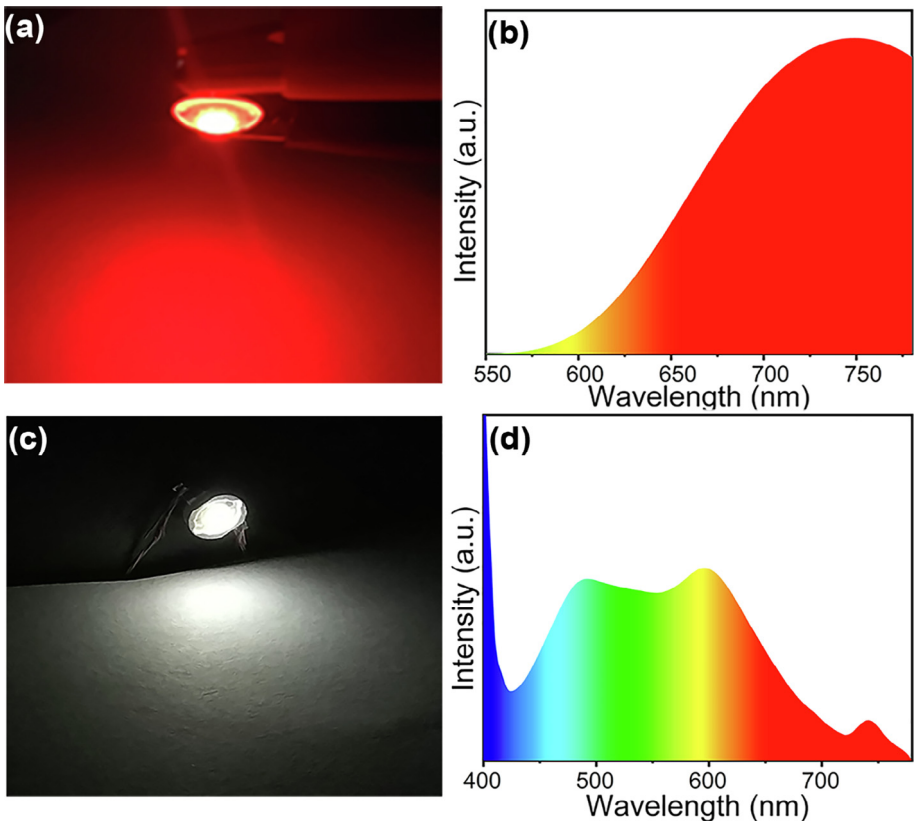

Fig. 6. CDs for LEDs. (a) The photograph of the working red LED, (b) emission spectrum, and (c) The photograph of the working white LED, (d) emission spectrum.

firstly incubated without Fe^{3+} ion at 37 °C, and laser scanning confocal microscopy images indicated that obvious red fluorescence was observed, suggesting that CDs successfully entered cells by endocytosis (Fig. 5c). Different concentrations of Fe^{3+} were added to MGC-803 cells pretreated with CDs to further study the application of CDs in the semi-quantitative detection of Fe^{3+} in cells. When the concentration of Fe^{3+} was 50 μmol L^{-1}, there was a significant decrease in the intracellular fluorescence (Fig. 5d), which may be due to a small amount of Fe^{3+} entering the cells. After increasing the concentration of Fe^{3+} to 100 and 250 μmol L^{-1}, the fluorescence decreased further, indicating that the quenching effect of CDs was better as the Fe^{3+} concentration increased (Fig. 5e and f). Thus, CDs can be used to visualize the monitoring of Fe^{3+} in living cells. Among them, the sensitivity and speed of sensing were much lower than that of aqueous solution, possibly because the inner and outer membrane of cells had higher Fe^{3+} adsorption capacity.

We also used CDs to prepare red and white LEDs. Composite nanocomposites were designed by polymerizing CDs in polymethyl methacrylate (PMMA) solution. PMMA/CDs were coated on 365 nm excitation light-emitting chips and cured in oven to form a solid-state lighting unit. The emission spectrum of the device (Fig. 6a, b) shows that the emission ranges of red PMMA/CDs phosphors ranges from 560 to 780 nm. The emission spectra of the LED devices showed an emission with CIE (Commission Internationale de L'Eclairage) color coordinates of (0.68, 0.31) and with the color rendering index (CRI) of 71.8 and color temperature of 1,000 K (Fig. S11 online). When mixed with the CDs we prepared before [29], we successfully designed the white LEDs (Fig. 6c, d) with CIE of (0.34, 0.37) (Fig. S11 online). The white LEDs show high CRI of 81.9 and color temperature of 4,957 K. We conclude that PMMA/CDs phosphors have good application value in future practical lighting applications.

3. Conclusions

In summary, we prepared near-infrared emissive CDs using a simple and low toxicity preparation process. The strongest emission of the CDs was observed centered at 685 nm with QY as high as 33.96% in aqueous solution. The as-prepared CDs were very stable after storing at room temperature for 40 days, and no quenching was observed in the 0–11 pH range. The as-prepared CDs exhibited good selectivity for Fe^{3+}, and we applied them for sensing the changes in the Fe^{3+} contents in living cells. Furthermore, the as-prepared CDs were also used in bioimaging and LEDs. The present work not only provided a new method for synthesizing aqueous-phase high QY near-infrared emissive CDs, but we also demonstrated the multifunctional applications of these CDs in living cell sensing and bioimaging applications.

Conflict of interest

The authors declare that they have no conflict of interest.

Acknowledgments

This work was financially supported by the China Postdoctoral Science Foundation (2018M640681, 2019T120632), the National Natural Science Foundation of China (21774041, 51433003) and the National Key Research and Development Program of China (2016YFB0401701).

Author contributions

Boyang Wang and Jian Li contributed to the synthesis and characterization. Boyang Wang wrote the manuscript. Zhiyong Tang

and Bai Yang supported and supervised the research. Siyu Lu conceived the idea and organized the manuscript. All the authors contributed to discussion.

Appendix A. Supplementary data

Supplementary data to this article can be found online at https://doi.org/10.1016/j.scib.2019.07.021.

References

[1] Hola K, Zhang Y, Wang Y, et al. Carbon dots-emerging light emitters for bioimaging, cancer therapy and optoelectronics. Nano Today 2014;9:590–603.
[2] Yuan F, Li S, Fan Z, et al. Shining carbon dots: synthesis and biomedical and optoelectronic applications. Nano Today 2016;11:565–86.
[3] Fernando KAS, Sahu S, Liu Y, et al. Carbon quantum dots and applications in photocatalytic energy conversion. ACS Appl Mater Interfaces 2015;7:8363–76.
[4] Meng W, Bai X, Wang B, et al. Biomass-derived carbon dots and their applications. Energy Environ Mater 2019. https://doi.org/10.1002/eem2.12038.
[5] Yan Y, Gong J, Chen J, et al. Recent advances on graphene quantum dots: from chemistry and physics to applications. Adv Mater 2019. https://doi.org/10.1002/adma.201808283.
[6] Lim SY, Shen W, Gao Z. Carbon quantum dots and their applications. Chem Soc Rev 2015;44:362–81.
[7] Peng Z, Han X, Li S, et al. Carbon dots: biomacromolecule interaction, bioimaging and nanomedicine. Coordin Chem Rev 2017;343:256–77.
[8] Liu ML, Chen BB, Li CM, et al. Carbon dots: synthesis, formation mechanism, fluorescence origin and sensing applications. Green Chem 2019;21:449–71.
[9] Zhang J, Yu S-H. Carbon dots: large-scale synthesis, sensing and bioimaging. Mater Today 2016;19:382–93.
[10] Mintz KJ, Zhou Y, Leblanc RM. Recent development of carbon quantum dots regarding their optical properties, photoluminescence mechanism, and core structure. Nanoscale 2019;11:4634–52.
[11] Du J, Xu N, Fan J, et al. Carbon dots for in vivo bioimaging and theranostics. Small 2019. https://doi.org/10.1002/smll.201805087.
[12] Qu D, Zheng M, Li J, et al. Tailoring color emissions from n-doped graphene quantum dots for bioimaging applications. Light-Sci Appl 2015;4. e364.
[13] Qu D, Miao X, Wang X, et al. Se & N co-doped carbon dots for high-performance fluorescence imaging agent of angiography. J Mater Chem B 2017;5:4988–92.
[14] Qu D, Yang D, Sun Y, et al. White emissive carbon dots actuated by the H-/J-aggregates and förster resonance energy transfer. J Phys Chem Lett 2019;10:3849–57.
[15] Ding H, Wei J-S, Zhang P, et al. Solvent-controlled synthesis of highly luminescent carbon dots with a wide color gamut and narrowed emission peak widths. Small 2018;14:1800612.
[16] Pan L, Sun S, Zhang A, et al. Truly fluorescent excitation-dependent carbon dots and their applications in multicolor cellular imaging and multidimensional sensing. Adv Mater 2015;27:7782–7.
[17] Guo S, Yang Y, Liu N, et al. One-step synthesis of cobalt, nitrogen-codoped carbon as nonprecious bifunctional electrocatalyst for oxygen reduction and evolution reactions. Sci Bull 2016;61:68–77.
[18] Zhang J, Dong L, Yu S-H. A selective sensor for cyanide ion (CN^-) based on the inner filter effect of metal nanoparticles with photoluminescent carbon dots as the fluorophore. Sci Bull 2015;60:785–91.
[19] Tian Z, Zhang X, Li D, et al. Full-color inorganic carbon dot phosphors for white-light-emitting diodes. Adv Opt Mater 2017;5:1700416.
[20] Miao X, Qu D, Yang D, et al. Synthesis of carbon dots with multiple color emission by controlled graphitization and surface functionalization. Adv Mater 2018;30:1704740.
[21] Ding H, Yu S-B, Wei J-S, et al. Full-color light-emitting carbon dots with a surface-state-controlled luminescence mechanism. ACS Nano 2015;10:484–91.
[22] Wu Z, Zhai Y, Kim H, et al. Emerging design and characterization guidelines for polymer-based infrared photodetectors. Acc Chem Res 2018;51:3144–53.
[23] Agostinis P, Berg K, Cengel KA, et al. Photodynamic therapy of cancer: an update. CA Cancer J Clin 2011;61:250–81.
[24] Nguyen V, Si J, Yan L, et al. Electron–hole recombination dynamics in carbon nanodots. Carbon 2015;95:659–63.
[25] Sun Y-P, Wang X, Lu F, et al. Doped carbon nanoparticles as a new platform for highly photoluminescent dots. J Phy Chem C 2008;112:18295–8.
[26] Li H, He X, Kang Z, et al. Water-soluble fluorescent carbon quantum dots and photocatalyst design. Angew Chem Int Ed 2010;49:4430–4.
[27] Bao L, Zhang Z-L, Tian Z-Q, et al. Electrochemical tuning of luminescent carbon nanodots: from preparation to luminescence mechanism. Adv Mater 2011;23:5801–6.
[28] Choi Y, Kang B, Lee J, et al. Integrative approach toward uncovering the origin of photoluminescence in dual heteroatom-doped carbon nanodots. Chem Mater 2016;28:6840–7.
[29] Yuan YH, Liu ZX, Li RS, et al. Synthesis of nitrogen-doping carbon dots with different photoluminescence properties by controlling the surface states. Nanoscale 2016;8:6770–6.
[30] Zhan Y, Geng T, Liu Y, et al. Near-ultraviolet to near-infrared fluorescent nitrogen-doped carbon dots with two-photon and piezochromic luminescence. ACS Appl Mater Interfaces 2018;10:27920–7.
[31] Zhang X, Jiang M, Niu N, et al. Natural-product-derived carbon dots: from natural products to functional materials. ChemSusChem 2018;11:11–24.
[32] Wei Z, Wang B, Liu Y, et al. Green synthesis of nitrogen and sulfur co-doped carbon dots from allium fistulosum for cell imaging. New J Chem 2019;43:718–23.
[33] Lu S, Zhao X, Zhu S, et al. Novel cookie-with-chocolate carbon dots displaying extremely acidophilic high luminescence. Nanoscale 2014;6:13939–44.
[34] Lu S, Cong R, Zhu S, et al. pH-dependent synthesis of novel structure-controllable polymer-carbon nanodots with high acidophilic luminescence and super carbon dots assembly for white light-emitting diodes. ACS Appl Mater Interfaces 2016;8:4062–8.
[35] Li W, Liu Y, Wu M, et al. Carbon-quantum-dots-loaded ruthenium nanoparticles as an efficient electrocatalyst for hydrogen production in alkaline media. Adv Mater 2018;30:1800676.
[36] Ghosal K, Ghosh A. Carbon dots: the next generation platform for biomedical applications. Mater Sci Eng C 2019;96:887–903.
[37] Chan KK, Yap SHK, Yong K-T. Biogreen synthesis of carbon dots for biotechnology and nanomedicine applications. Nano-Micro Lett 2018;10:72.
[38] Song Y, Zhu C, Song J, et al. Drug-derived bright and color-tunable N-doped carbon dots for cell imaging and sensitive detection of Fe^{3+} in living cells. ACS Appl Mater Interfaces 2017;9:7399–405.
[39] Shen P, Xia Y. Synthesis-modification integration: one-step fabrication of boronic acid functionalized carbon dots for fluorescent blood sugar sensing. Anal Chem 2014;86:5323–9.
[40] Shangguan J, He D, He X, et al. Label-free carbon-dots-based ratiometric fluorescence pH nanoprobes for intracellular pH sensing. Anal Chem 2016;88:7837–43.
[41] Jiang Y, Wang Z, Dai Z. Preparation of silicon–carbon-based dots@dopamine and its application in intracellular Ag^+ detection and cell imaging. ACS Appl Mater Interfaces 2015;8:3644–50.
[42] Chen T-H, Tseng W-L. Self-assembly of monodisperse carbon dots into high-brightness nanoaggregates for cellular uptake imaging and iron(iii) sensing. Anal Chem 2017;89:11348–56.
[43] Li W, Liu Y, Wang B, et al. Kilogram-scale synthesis of carbon quantum dots for hydrogen evolution, sensing and bioimaging. Chin Chem Lett 2019. https://doi.org/10.1016/j.cclet.2019.06.040.
[44] Yuan F, Yuan T, Sui L, et al. Engineering triangular carbon quantum dots with unprecedented narrow bandwidth emission for multicolored LEDs. Nat Commun 2018;9:2249.
[45] Zhang M, Su R, Zhong J, et al. Red/orange dual-emissive carbon dots for pH sensing and cell imaging. Nano Res 2019;12:815–21.
[46] Wang Z, Yuan F, Li X, et al. 53% efficient red emissive carbon quantum dots for high color rendering and stable warm white-light-emitting diodes. Adv Mater 2017;29:1702910.
[47] Miao X, Yan X, Qu D, et al. Red emissive sulfur, nitrogen codoped carbon dots and their application in ion detection and theraonostics. ACS Appl Mater Interfaces 2017;9:18549–56.
[48] Wang Q, Zhang S, Wang B, et al. Pressure-triggered aggregation-induced emission enhancement in red emissive amorphous carbon dots. Nanoscale Horiz 2019. https://doi.org/10.1039/C9NH00287A.
[49] Qu D, Sun Z, Zheng M, et al. Three colors emission from S, N co-doped graphene quantum dots for visible light H_2 production and bioimaging. Adv Opt Mater 2015;3:360–7.
[50] Xu J, Jie X, Xie F, et al. Flavonoid moiety-incorporated carbon dots for ultrasensitive and highly selective fluorescence detection and removal of Pb^{2+}. Nano Res 2018;11:3648–57.
[51] Liu Y, Duan W, Song W, et al. Red emission B, N, S-co-doped carbon dots for colorimetric and fluorescent dual mode detection of Fe^{3+} ions in complex biological fluids and living cells. ACS Appl Mater Interfaces 2017;9:12663–72.
[52] Gao W, Song H, Wang X, et al. Carbon dots with red emission for sensing of Pt^{2+}, Au^{3+}, and Pd^{2+} and their bioapplications in vitro and in vivo. ACS Appl Mater Interfaces 2017;10:1147–54.
[53] Liu J, Li D, Zhang K, et al. One-step hydrothermal synthesis of nitrogen-doped conjugated carbonized polymer dots with 31% efficient red emission for in vivo imaging. Small 2018;14:1703919.
[54] Lu S, Sui L, Wu M, et al. Graphitic nitrogen and high-crystalline triggered strong photoluminescence and room-temperature ferromagnetism in carbonized polymer dots. Adv Sci 2019;6:1801192.
[55] Lu S, Sui L, Liu J, et al. Near-infrared photoluminescent polymer-carbon nanodots with two-photon fluorescence. Adv Mater 2017;29:1603443.
[56] Li F, Yang D, Xu H. Non-metal-heteroatom-doped carbon dots: synthesis and properties. Chem Eur J 2019;25:1165–76.
[57] Yang Q, Duan J, Yang W, et al. Nitrogen-doped carbon quantum dots from biomass via simple one-pot method and exploration of their application. Appl Surf Sci 2018;434:1079–85.
[58] Zhang Z, Shi Y, Pan Y, et al. Quinoline derivative-functionalized carbon dots as a fluorescent nanosensor for sensing and intracellular imaging of Zn^{2+}. J Mater Chem B 2014;2:5020–7.

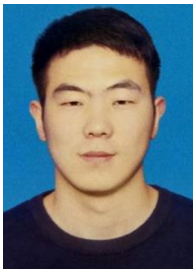

Boyang Wang obtained his B.S. degree in College of Chemistry and Chemical Engineering, Lanzhou University in 2018. He is currently a M.S. student under the supervision of Prof. Siyu Lu at Zhengzhou University. His research is centered on the synthesis and application of Carbonized Polymer Dots.

Siyu Lu is currently an associate professor of College of Chemistry and Molecular Engineering, Zhengzhou University. He received his Ph.D. degree in polymer physics and chemistry under the supervision of Prof. Bai Yang at Jilin University. His research interests relate to the design, preparation, properties of photoelectric nanocrystals (Carbon dots, Semiconductors, etc.) and their applications in catalysis, superconductivity, thermoelectricity, and structural prediction.